Article

A Performance Analysis on Soil Dielectric Models Over Organic Soils in Alaska for Passive Microwave Remote Sensing of Soil Moisture

Runze Zhang [1,*], Steven Chan [2], Rajat Bindlish [3] and Venkataraman Lakshmi [1]

[1] Department of Engineering Systems and Environment, University of Virginia, Charlottesville, VA 22904; vlakshmi@virginia.edu
[2] NASA Jet Propulsion Laboratory, California Institute of Technology, Pasadena, CA 91109, USA; steventsz.k.chan@jpl.nasa.gov
[3] NASA Goddard Space Flight Center, Greenbelt, MD 20771, USA; rajat.bindlish@nasa.gov
* Correspondence: rz4pd@virginia.edu

Abstract: Passive microwave remote sensing of soil moisture (SM) requires a physically based dielectric model that quantitatively converts the volumetric SM into the soil bulk dielectric constant. Mironov 2009 is the dielectric model used in the operational SM retrieval algorithms of the NASA Soil Moisture Active Passive (SMAP) and the ESA Soil Moisture and Ocean Salinity (SMOS) missions. However, Mironov 2009 suffers a challenge in deriving SM over organic soils as it does not account for the impact of soil organic matter (SOM) on the soil bulk dielectric constant. To this end, we presented a comparative performance analysis of nine advanced soil dielectric models over organic soil in Alaska and four of them incorporate SOM. In the framework of the SMAP single-channel algorithm at vertical polarization (SCA-V), SM retrievals from different dielectric models were derived using an iterative optimization scheme. The skills of different dielectric models over organic soils were reflected by the performance of their respective SM retrievals, which was measured by four conventional statistical metrics calculated by comparing satellite-based SM time series with in-situ benchmarks. Overall, SM retrievals of organic-soil-based dielectric models tended to overestimate while those from mineral-soil-based models displayed dry biases. All the models showed comparable values of unbiased root-mean-square error (ubRMSE) and Pearson Correlation (R), but Mironov 2019 exhibited a slight and consistent edge over others. An integrated consideration of the model inputs, the physical basis, and the validated accuracy indicated that the separate use of Mironov 2009 and Mironov 2019 in the SMAP SCA-V for mineral soils (SOM $<$ 15%) and organic soils (SOM $\geq$ 15%) would be a preferred option.

Keywords: Soil Moisture; Dielectric Models; SMAP; Soil Organic Matter

1. Introduction

Passive microwave remote sensing is considered the most suitable tool to map spatial soil wetness owing to the negligible atmospheric influence and less interference from canopy and surface roughness [1,2]. The remarkable performance of soil moisture (SM) retrievals from spaceborne L-band radiometers (i.e., Soil Moisture and Ocean Salinity (SMOS) [3] and Soil Moisture Active Passive (SMAP) [4]) has been substantiated by a number of validation studies [5-9]. The mechanism that physically bridges the surface emission at microwave bands and surface SM is based on the contrasting difference between the dielectric constants of liquid water (~ 80) and dry soil (~ 4) [10]. The dielectric model that quantitatively links the SM with the bulk dielectric constant of the soil-water-air system is therefore critical in the retrieval algorithms of SMOS and SMAP.

Recently, numerous dielectric models were developed and applied for both spaceborne microwave radiometers and in-situ electromagnetic sensors [11]. An ideal dielectric model is envisioned to accurately account for the dielectric response of wet soils as a function of all the relevant factors, including soil compaction, soil composition, the fraction of bound and free water, salinity, soil temperature, soil particle size distribution, and observation frequency, etc. [12]. However, the practical dielectric models are often established on a limited set of soil properties and are unable to approximate proper dielectric constants for all the surface conditions. Previous studies found that applying mineral-soil-based dielectric models over organic soils could lead to a substantial underestimation of SM [11]. [13] revealed a significant drop in the SMAP retrieval quality in regions with soil organic carbon (SOC) exceeding 8.72%. Given that Mironov 2009 [14] currently used in the SMOS and SMAP operation algorithms, was developed exclusively on samples of mineral soils, an update on the dielectric model that incorporates the effect of soil organic matter (SOM) is pressingly required for areas with organic-rich soils.

The influence of SOM on the bulk dielectric constant of the soil-water system is often summarized in two aspects. First, organic substrates have larger specific surface areas than minerals, indicating that organic soil has a higher fraction of bound water relative to mineral soil when they contain the same amount of water [11,15,16]. As such, at the same moisture, the dielectric constant of organic soil tends to be lower than that of mineral soil as the dielectric constant of bound water is much smaller than that of free water. Second, organic soil is often marked with a larger porosity than mineral soil due to its complex structure [11,15-17]. Based on these principles, several organic-soil-based dielectric models have been developed in recent years.

Although model developers pointed out the potential applicability of their models in the retrieval of SM, assessment of the efficacy of these newly developed organic-soil-based dielectric models in the derivation of passive microwave remote sensing of SM, has not been widely carried out. In light of these, nine advanced dielectric mixing models were selected and tested in the context of the SMAP single-channel algorithm at vertical polarization (SCA-V) [18]. This study has two major objectives: 1) present the differences between the available mineral- and organic-soil-based models in describing the complex dielectric behaviors of wet soils under various SOM conditions, and 2) evaluate their performances in organic-rich soils. The latter was achieved by comparing the SCA-V SM retrievals from different models against in-situ measurements scattered over Alaska where the soils are identified with noticeably higher SOM (~ 25%) relative to the global average level (**Figure A1**). The dielectric models considered here have been classified as the mineral-soil-based dielectric models, including Wang 1980 [19], the semi-empirical Dobson 1985 modified by Peplinski 1995 [12,20] (hereafter Dobson 1985), the prevalent Mironov 2009 [14], Mironov 2012 [21], and Park 2017 [22], and organic-soil-based dielectric models, including the natural log fitting model in [11] (hereafter Bircher 2016), Mironov 2019 [23], Park 2019 [16], and Park 2021 [24].

The paper is organized as follows. In Section 2, all the data sets and the preprocessing steps are presented. The followings are the workflow of in-situ measurements screening and the partial SMAP SCA-V retrieval process used to derive SM from the identical observation and different models (Section 3). The results of synthetic experiments, validation consequences over Alaska, and a detailed discussion are subsequently displayed in Section 4. Finally, conclusions are followed by a brief summary presented in Section 5.

2. Data

2.1. SMAP L2 Radiometer Half-Orbit 36km EASE-Grid Soil Moisture, Version 8

Launched on January 31, 2015, the SMAP mission was designed to map high-resolution SM and freeze/thaw state by combining the attributes of L-band radar and radiometer. However, the SMAP SM products presently rely on the radiometer's observations alone due to an unexpected malfunction of the SMAP radar in July 2015. With an average revisit frequency of two to three days, the SMAP sensors cross the Equator at the local solar time of 6 a.m. and 6 p.m.

SMAP L2 Radiometer Half-Orbit 36 km EASE-Grid Soil Moisture, Version 8 (SMAP V8) [25] was adopted in this study. Here, we only used the descending (6 a.m.) SM retrievals derived using the SCA-V algorithm. A series of masking procedures were utilized to avoid the applications of SM retrievals of low accuracy and high uncertainty. Specifically, only the retrievals flagged as the 'recommended quality' were retained and employed in the later analysis. A threshold of 4 ºC based on in-situ temperature observations has also been selected to filter out those SM measurements likely obtained during a period of active thawing and re-freezing (e.g., **Figure 3c** in [26]) . Given Alaska, the focused region of this study, locates at the high-latitude portion with a long-term frozen duration, we only considered those qualified SM retrievals within the time intervals from June to August between 2015 and 2021.

One noticeable improvement in the SMAP V8 (relative to an older version) is the update and extension of gridded soil parameters, ranging from SOC, silt and sand fraction to bulk density. These newly added soil attributes originate from the SoilGrid 250m [27] and replace the earlier patched version composed of the National Soil Data Canada (NSDC), the State Soil Geographic Database (STATSGO), the Australia Soil Resources Information System (ASRIS), and the Harmonized World Soil Database (HWSD) [28]. Since these soil attributes are often necessary inputs for dielectric models of soil, they were also extracted from the SMAP V8.

2.2. in-situ Soil Moisture Measurements

Ground-based SM measurements over Alaska were employed as benchmarks to assess the skills of diverse dielectric mixing models. Historical files of soil water content observed by in-situ sensors were first downloaded from the Natural Resources Conservation Service (NRCS), the National Water and Climate Center (NWCC) homepage (https://www.nrcs.usda.gov/wps/portal/wcc/home). At present, there are more than 40 operating stations from the Snow Telemetry (SNOTEL) [29] and Soil Climate and Analysis Network (SCAN) [30]. These stations are able to monitor the sub-daily variations of SM and many other climatic variables in near-real time.

However, some typical errors [26] of in-situ SM readings, such as breaks and plateaus, have been found before their application. As a response, the other authoritative data source of in-situ SM, the International Soil Moisture Network (ISMN) [31,32], was also considered, aiming at incorporating its flag information. Given the limited stations in Alaska, it is expected that SM data from the above two sources (NWCC and ISMN) are mostly from the same set of stations. Additionally, for the same station, the observed SM time series from the NWCC and ISMN should be identical as the ISMN only gathers data and harmonizes them in units and time steps without extra data processing. Given the frequent abnormal SM readings (even after adopting the quality flag) and the necessity of checking the consistency of SM measurements from two different sources, several rigorous pre-checking procedures were applied (as described in Section 3.1) to filter out those suspicious observations where possible in advance.

3. Methodology

3.1. Preliminary Examination of in-situ Measurements

The quality of in-situ SM data is of great importance as these ground measurements are generally seen as the benchmark for evaluating remotely sensed and/or modeled SM data sets [5-7]. However, monitoring SM dynamics over high-latitude regions is still challenging due to the long-term frozen periods and harsh environments. Such difficulties have been reflected by the flat limbs and breaks frequently occurring in the SM time series from the Alaskan stations. Given those, a careful examination of in-situ SM measurements is necessary.

The general workflow of the preliminary examination steps is delineated in **Figure 1**. Specifically, the in-situ SM data measured at the local time of 6 a.m. and 6 p.m. (temporally align with the SMAP overpass time) were first extracted from the NWCC and ISMN's stations. Like the SMAP SM pre-processing, SM measurements with the corresponding land surface temperature below 4 ºC were excluded. Additionally, stations with a distance shorter than 36 km to large water bodies or oceans were also masked as the SMAP SM over those regions is likely influenced by water contamination. The flag information from the ISMN was also incorporated to filter in-situ data of low quality.

The matched SM data of the overlapped stations from the NWCC and ISMN are anticipated, and the greater consistency further enhances the reliability of these benchmarks. Therefore, an automatic consistency checking procedure constrained by three requirements was applied. Since breaks and plateaus still appeared on the SM time series after consistency checking, a manual visual inspection was then performed to screen those suspicious measurements. After those, there are 21 qualified stations left, and we assume that their SM data from the NWCC and ISMN are interchangeable. Furthermore, pairing with the SMAP observations removed 9 stations, and the remaining 12 stations (**Figure S1**) would be used in the later validation steps.

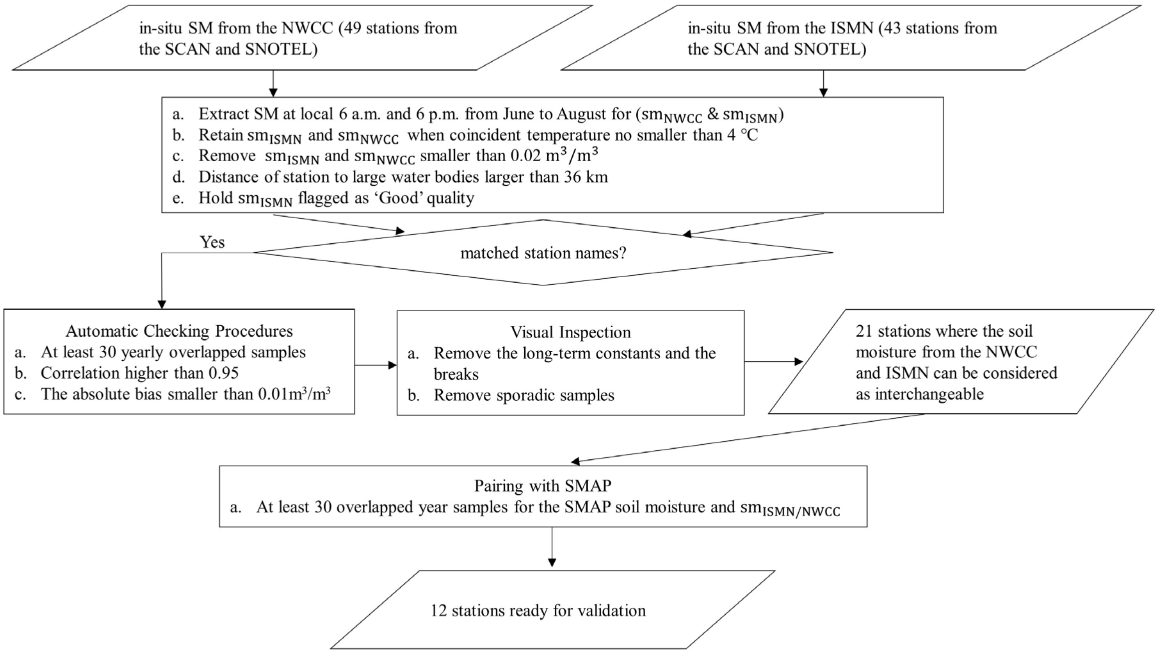

Figure 1. The flow chart of the preliminary examination on the Alaskan in-situ soil moisture obtained from the NWCC and ISMN

3.2. Derivation of Soil Moisture from Various Dielectric Models

In the SCA-V algorithm, SMAP SM value is finally determined when there is a minimized difference between the simulated and the observed reflectivity (r_{smap}) (reflectivity = 1 – emissivity) of smooth soil. At each temporal step, the value of r_{smap} over a pixel is fixed as SMAP SCA algorithm have determined the radiative contribution from the canopy layer and the impact of surface roughness before subtracting them from SMAP observed surface brightness temperature (T_B). Hence, the influence of adopting different dielectric constant models on SM retrievals can be examined using the iterative feedback-loop procedure to minimize the difference between the simulated reflectivity (r_{est}) and r_{smap} and without the need to construct the whole process from SM to T_B in consideration of simplicity.

However, r_{smap} is an intermediate product and unavailable from the original SMAP data set. Given this, the values of r_{smap} were first estimated leveraging SMAP SM and Mironov 2009. With these benchmarks, the SM retrievals of other dielectric models were then acquired based on the optimization flow described in **Figure 2**. Notably, the SM retrieval at a given time point is reproducible while the identical r_{smap} and model are used.

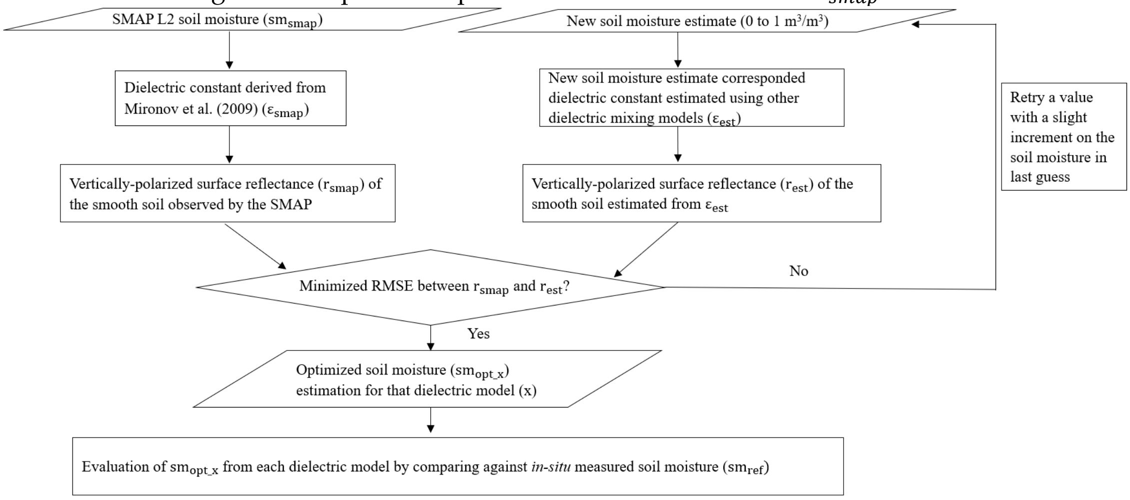

Figure 2. Flow chart that describes the retrieval of soil moisture using different dielectric models based on the identical SMAP observations.

3.3. Performance Metrics

The skill of the remote sensing SM data set has been described by four conventional metrics, which are bias, root-mean-square error (RMSE), unbiased root-mean-square error (ubRMSE), and the Pearson correlation (R) [33]. These metrics could effectively reflect the discrepancies in terms of magnitudes as well as the links of the temporal evolutions between the SM estimations and the ground truth. The formulas used to compute these metrics are shown from Eq 1 to Eq 4 where E [...] represents the arithmetic mean; σ_{opt} and σ_{ref} denote the standard deviations of SM retrievals of the respective dielectric model and in-situ measured SM.

$$\mathrm{bias} = \mathrm{E}[\mathrm{sm_{ret}}] - \mathrm{E}[\mathrm{sm_{ref}}] \tag{1}$$

$$\mathrm{RMSE} = \sqrt{\mathrm{E}[(\mathrm{sm_{ret}} - \mathrm{sm_{ref}})^2]} \tag{2}$$

$$\mathrm{ubRMSE} = \sqrt{\mathrm{RMSE}^2 - \mathrm{bias}^2} \tag{3}$$

$$\mathrm{R} = \frac{\mathrm{E}[(\mathrm{sm_{ret}} - \mathrm{E}[\mathrm{sm_{ret}}])(\mathrm{sm_{ref}} - \mathrm{E}[\mathrm{sm_{ref}}])]}{\sigma_{\mathrm{ret}}\sigma_{\mathrm{ref}}} \tag{4}$$

4. Results and Discussion

4.1. Simulated Brightness Temperature of Smooth Soil through Synthetic Experiments

Synthetic experiments have the capability to afford complete dielectric responses to a whole SM range by artificially controlling all the inputs required for the dielectric models (**Table 1**). With SOM increasing from 0% to 75% at a step of 15%, the differences between the dielectric constants estimated by mineral- and organic-soil-based dielectric models were explored. These various dielectric responses were further transferred to their corresponding thermal radiations of smooth soils, represented by the vertically polarized T_B.

Figure 3 presents the T_B curves derived using different dielectric models across the range of SM from 0 to 0.8 m³/m³. Generally, T_B values estimated using organic-soil-based models are greater than those derived using the mineral-soil-based models particularly when SOM exceeds 15% and SM is higher than 0.1 m^3/m^3. In other words, SM retrievals from organic-soil-based models tend to be wetter than the SM retrievals from mineral-soil-based models (e.g., Mironov 2009) given the same surface reflectivity (or T_B) of bare, smooth soil. The discrepancies between the simulated T_B magnitudes from mineral- and organic-soil-based models further grow with the increase of SOM (**Figure 3**). However, it should be noted that the estimated dielectric constants and their subsequent T_B values from mineral-soil-based models do not vary with SOM. The higher SM estimations of organic-soil-based models relative to mineral-soil-based models could be attributed to the fact that those organic-soil-based models assume a higher volumetric proportion of bound water [11,15,16].

When SOM is at 15% (and below), the simulated T_B curves from all the considered models are clustered together, bounded by Dobson 1985 and Bircher 2016 (**Figure 3b**). Therefore, SOM of 15% might be treated as an appropriate demarcation point for the separate use of mineral- and organic-soil-based dielectric models over mineral soils and organic soils. Similar features of the T_B curves of those considered dielectric models have been observed while a sandy sample is tested (**Figure S2**).

Compared to Mironov 2019, the influence of organic content on the simulated T_B magnitude seems more pronounced for Park 2019 and Park 2021. When SOM increases from 0% to 75% and SM values are smaller than 0.5 m^3/m^3, the T_B curve of Park 2021 jumps from the bottom one to the top line, with a varying amplitude on the order of tens of Kelvins (**Figure 3**). In contrast, as a response to growing SOM, the estimations from Mironov 2019 slowly move upward approaching the T_B curve of Bircher 2016. According to **Figure 3e and f**, there is a rapidly dropping segment on the T_B curve of Park 2019. Such abnormal dielectric behavior can be attributed to the improper formulas used to calculate the wilting point and porosity, with a detailed explanation in Section 4.4.

Table 1. Input variables required for nine dielectric models.

Model Inputs	Mineral Soil Based Models					Organic Soil Based Models			
	Wang 1980	Dobson 1985	Mironov 2009	Mironov 2013	Park 2017	Bircher 2016	Mironov 2019	Park 2019	Park 2021
Soil Moisture	Volumetric Soil Moisture (m^3/m^3)	Volumetric Soil Moisture (m^3/m^3)	Volumetric Soil Moisture (m^3/m^3)	Volumetric Soil Moisture (m^3/m^3)	Volumetric Soil Moisture (m^3/m^3)	Volumetric Soil Moisture (m^3/m^3)	Gravimetric Soil Moisture (g/g)	Volumetric Soil Moisture (m^3/m^3)	Volumetric Soil Moisture (m^3/m^3)
Soil Organic Matter	/	/	/	/	/	/	Gravimetric Soil Organic Matter (%)	Gravimetric Soil Organic Matter (%)	Gravimetric Soil Organic Matter (%)
Clay	Gravimetric Clay Fraction (0-1)	Gravimetric Clay Fraction (0-1)	Gravimetric Clay Fraction (%)	Gravimetric Clay Fraction (%)	Volumetric Clay Fraction (0-1)	/	/	Volumetric Clay Fraction (0-1)	Volumetric Clay Fraction (0-1)
Sand	Gravimetric Sand Fraction (0-1)	Gravimetric Sand Fraction (0-1)	/	/	Volumetric Sand Fraction (0-1)	/	/	Volumetric Sand Fraction (0-1)	Volumetric Sand Fraction (0-1)
Silt	/	/	/	/	Volumetric Silt	/	/	Volumetric Silt	Volumetric Silt

					Fraction (0-1)			Fraction (0-1)	Fraction (0-1)
Bulk Density	Bulk Density (g/cm³)	Bulk Density (g/cm³)	/	/	/	/	Bulk Density (g/cm³)	/	/
Frequency	/	Frequency (Hz)	Frequency (Hz)	/	Frequency (Hz)	/	/	Frequency (Hz)	Frequency (Hz)
Salinity	/	/	/	/	Salinity (‰)	/	/	Salinity (‰)	Salinity (‰)
Soil Temperature	/	Soil Temperature (°C)	/	Soil Temperature (°C)	Soil Temperature (°C)	/	Soil Temperature (°C)	Soil Temperature (°C)	Soil Temperature (°C)
Total Number of Inputs	4	6	3	3	7	1	4	8	8

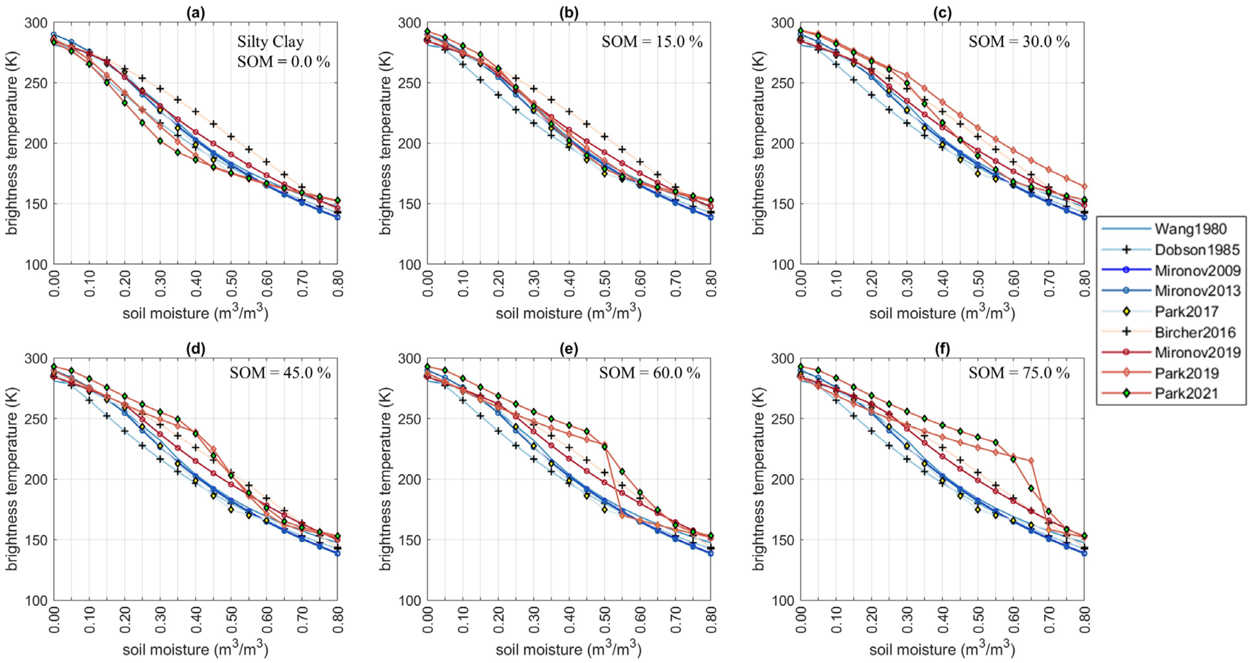

Model Inputs	Gravimetric Sand Fraction (%)	Gravimetric Clay Fraction (%)	Gravimetric Silt Fraction (%)	Bulk Density (g/cm³)	Salinity (‰)	Soil Physical Temperature (°C)	Frequency (GHz)	Soil Organic Matter (%)	Volumetric Soil Moisture (m³/m³)	Incidence Angle (°)
Simulated Values	5.0	47.6	47.4	1.42	0.0	20.0	1.4	0.0, 15.0, 30.0, 45.0, 60.0, 75.0	0.0 – 0.8	40.0

Figure 3. Simulated brightness temperature of a silty clay with various soil organic matter, and the accompanied table displays all the input values where most of soil parameters are directly taken from the sample of silty clay used in [34].

4.2. Evaluation of Dielectric Models over in-situ Sites in Alaska

Here, SM measurements from 12 sites served as benchmarks to evaluate the skills of multiple dielectric models in the setting of SMAP observations and its SCA-V algorithm. Before inter-comparison, it has been found that the assessment metrics of the satellite-based SM retrievals over the same pixel could vary a lot in different years. Using the time series in Monument Creek as an instance (**Figure 4**), R values range from 0.18 (2017) to 0.69 (2015). Hence, the obtained metrics (**Table 2**, **Table 3**, and **Table 4**) averaged over multiple years of each station might be underrated as they may be compromised by abnormal behavior in one year. Additionally, the amplitudes and frequencies of in-situ SM variations are often more pronounced relative to the SM retrievals as the latter reflects the changes over a coarse spatial extent (**Figure 4**).

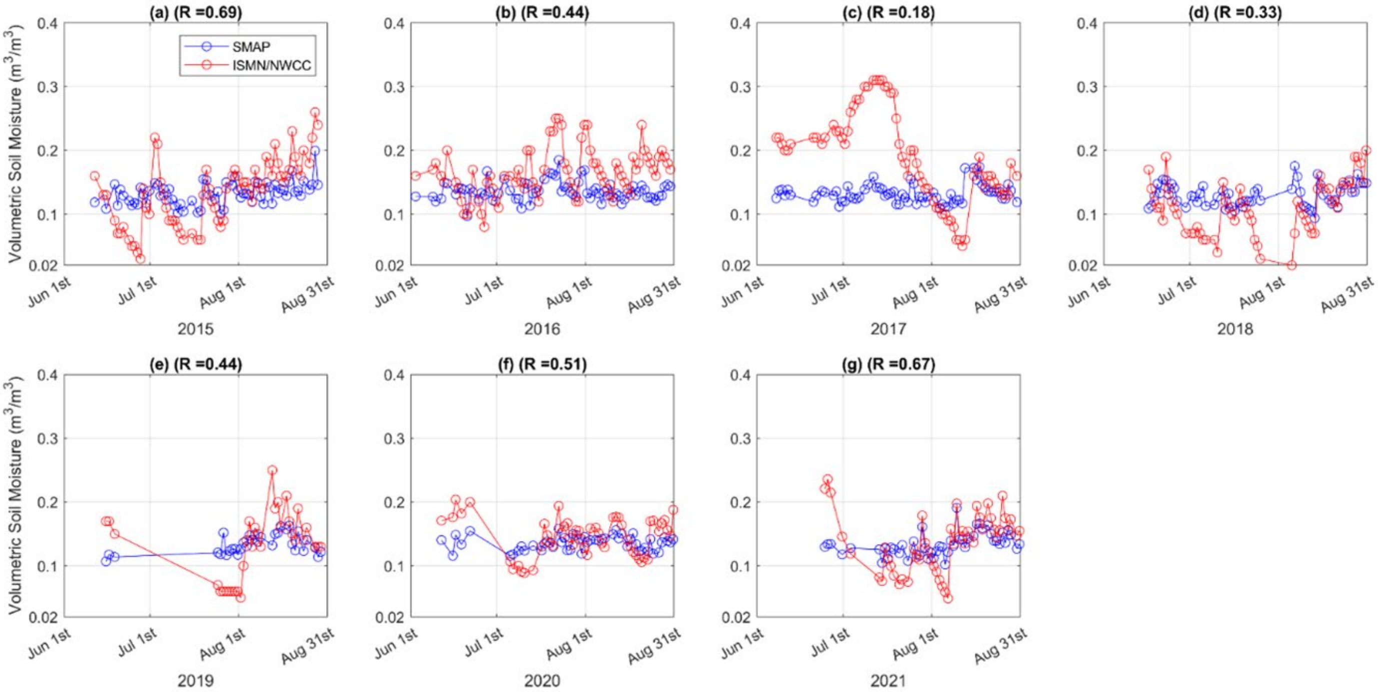

Figure 4. Time series of soil moisture derived from satellite observations and *in-situ* measurements at Monument Creek (65.18º N, 145.87º W).

Assessment metrics of the SM retrievals derived using identical r_{smap} values and different dielectric models were computed by their temporally paired in-situ measurements. According to **Table 2**, SM estimates from mineral-soil-based models tend to underestimate while organic-soil-based models generally exhibit wet biases compared to ground recordings. In terms of both ubRMSE and R (**Table 3** and **Table 4**), all the models show comparable accuracy levels similar to previous results of [35] whereas Mironov 2019 displays a slight but consistent edge over other models. Compared to other dielectric models, the modest improvement in R of Mironov 2019 is likely due to its simultaneous consideration of bulk density and SOM effects [23].

The other aspect that we attempted to evaluate the predictive power of various dielectric models was checking the correlations between the SM retrievals of different models and SMAP observed vertically polarized T_B. If the higher absolute R values between the time series of SM and SMAP vertically polarized T_B are assumed as a criterion that reflects the better skill of a dielectric mixing model, Mironov 2019 presents an overwhelming superiority over other models in the 765 Alaskan pixels (**Figure 5**). Table SX displays that in-situ measured SM usually has a lower correlation with SMAP vertically polarized T_B relative to correlations between satellite-based SM retrievals and SMAP T_B. However, it should be noted that such correlation-based results were inconclusive and functioned as a reference only since the impacts of vegetation disturbance and surface roughness were entirely ignored.

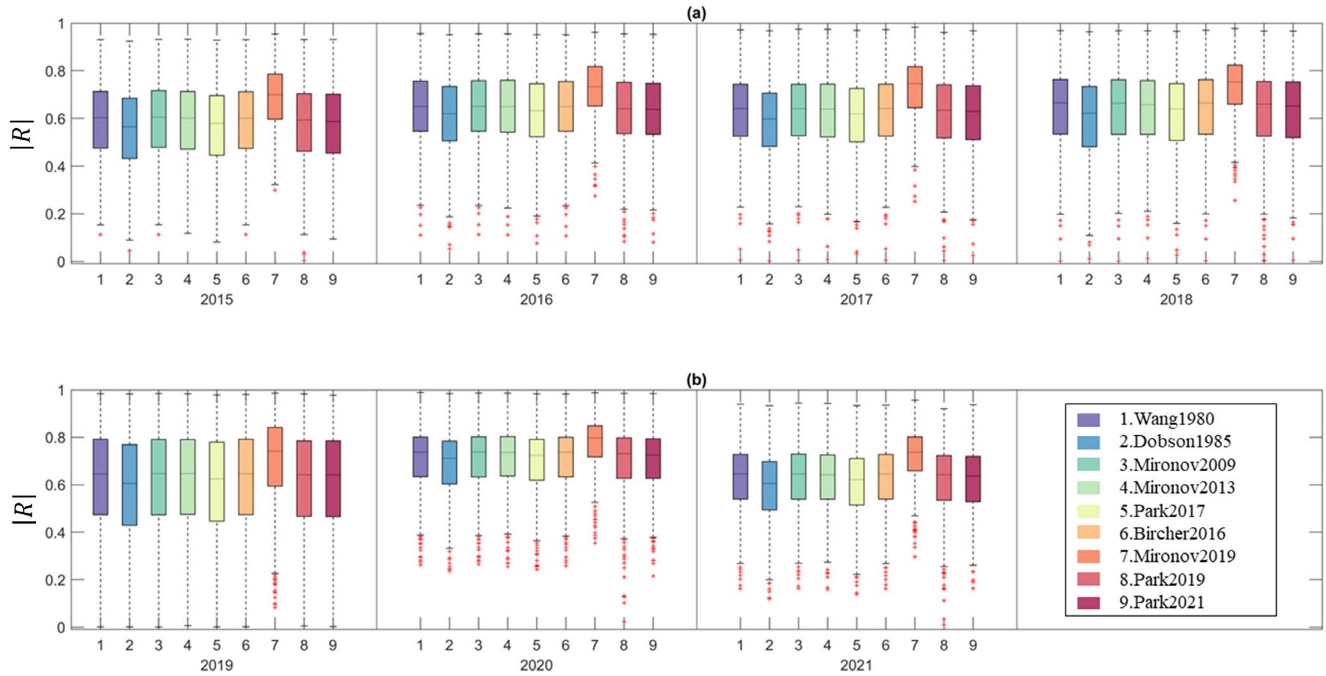

Figure 5. Boxplots of the absolute correlations between the soil moisture retrievals from various dielectric mixing models and the SMAP vertically polarized brightness temperature over the 765 pixels in Alaska.

Table 2. Bias of soil moisture retrievals using various dielectric models over in-situ sites in Alaska where biases from mineral- and organic-soil based models tend to underestimate and overestimate relative to in-situ measurements.

Station/Bias (m^3/m^3)	N	Mineral Soil Based Models					Organic Soil Based Models			
		Wang1980	Dobson 1985	Mironov 2009	Mironov 2013	Park 2017	Bircher 2016	Mironov 2019	Park 2019	Park 2021
Gulkana River	72	0.058	**0.025**	0.046	0.044	0.039	0.195	0.142	0.104	0.085
Spring Creek	37	-0.108	-0.153	-0.137	-0.137	-0.139	**-0.022**	-0.051	-0.105	-0.109
Atigun Pass	81	0.047	**-0.002**	0.015	0.016	0.009	0.092	0.092	0.044	0.061
Coldfoot	156	-0.085	-0.133	-0.121	-0.121	-0.124	**-0.030**	-0.036	-0.083	-0.067
Eagle Summit	320	-0.028	-0.068	-0.062	-0.061	-0.068	**0.014**	0.017	-0.033	-0.015
Gobblers Knob	262	0.031	-0.010	**-0.003**	-0.003	-0.007	0.096	0.083	0.039	0.055
Monahan Flat	121	-0.047	-0.093	-0.076	-0.077	-0.081	0.035	**0.009**	-0.029	-0.029
Monument Creek	405	0.018	-0.022	**-0.014**	-0.014	-0.016	0.091	0.073	0.029	0.041
Mt. Ryan	194	0.114	**0.078**	0.082	0.082	0.080	0.196	0.172	0.132	0.142
Munson Ridge	383	0.018	-0.019	**-0.015**	-0.015	-0.016	0.096	0.075	0.034	0.045
Tokositna Valley	253	0.014	-0.008	**-0.006**	-0.008	-0.008	0.147	0.093	0.062	0.046
Upper Nome Creek	283	-0.138	-0.180	-0.171	-0.171	-0.176	**-0.086**	-0.091	-0.138	-0.120
Mean	214	-0.009	-0.049	-0.038	-0.039	-0.042	0.069	0.048	**0.005**	0.011

Where the column of the number tagged by bold font represents the dielectric model with the smallest absolute bias in that station or mean.

Table 3. ubRMSE of soil moisture retrievals using various dielectric models over in-situ sites in Alaska.

Station/ubRMSE (m^3/m^3)	N	Mineral Soil Based Models					Organic Soil Based Models			
		Wang 1980	Dobson 1985	Mironov 2009	Mironov 2013	Park 2017	Bircher 2016	Mironov 2019	Park 2019	Park 2021
Gulkana River	72	**0.0132**	0.0164	0.0156	0.0154	0.0152	0.0209	0.0180	0.0169	0.0138
Spring Creek	37	0.0460	0.0457	0.0452	0.0454	0.0455	**0.0408**	0.0428	0.0446	0.0462
Atigun Pass	81	0.0311	0.0311	0.0311	0.0311	0.0311	0.0317	0.0311	0.0310	**0.0310**
Coldfoot	156	0.0736	0.0736	0.0736	0.0736	**0.0736**	0.0743	0.0737	0.0739	0.0737
Eagle Summit	320	0.0487	0.0490	0.0487	0.0487	0.0487	0.0480	**0.0477**	0.0482	0.0481
Gobblers Knob	262	0.0665	0.0663	0.0660	0.0662	0.0662	**0.0622**	0.0643	0.0628	0.0637
Monahan Flat	121	0.0722	0.0721	0.0720	0.0721	0.0721	**0.0714**	0.0718	0.0715	0.0722
Monument Creek	405	0.0510	0.0509	0.0508	0.0508	0.0508	0.0505	0.0503	0.0504	**0.0503**
Mt. Ryan	194	**0.0163**	0.0177	0.0173	0.0172	0.0173	0.0262	0.0186	0.0237	0.0187
Munson Ridge	383	0.0499	0.0492	0.0490	0.0492	0.0492	**0.0465**	0.0475	0.0467	0.0478
Tokositna Valley	253	0.1295	0.1296	0.1295	0.1295	0.1296	0.1298	**0.1294**	0.1296	0.1296
Upper Nome Creek	283	**0.0122**	0.0126	0.0124	0.0123	0.0126	0.0196	0.0129	0.0163	0.0160
Mean	214	0.0509	0.0512	0.0509	0.0510	0.0510	0.0518	**0.0507**	0.0513	0.0509

Where the column of the number tagged by bold font represents the dielectric model with the best ubRMSE in that station or mean.

Table 4. R of soil moisture retrievals using various dielectric models over in-situ sites in Alaska.

Station/R	N	Mineral Soil Based Models					Organic Soil Based Models			
		Wang 1980	Dobson 1985	Mironov 2009	Mironov 2013	Park 2017	Bircher 2016	Mironov 2019	Park 2019	Park 2021
Gulkana River	72	0.605	0.596	0.607	0.604	0.599	0.608	**0.621**	0.603	0.601
Spring Creek	37	0.757	0.737	0.758	0.752	0.745	0.757	**0.805**	0.752	0.746
Atigun Pass	81	0.342	**0.348**	0.344	0.344	0.344	0.341	0.333	0.347	0.347
Coldfoot	156	0.205	0.205	0.204	0.204	0.205	0.206	0.199	0.202	**0.208**
Eagle Summit	320	0.375	0.353	0.372	0.376	0.368	0.376	**0.429**	0.368	0.372
Gobblers Knob	262	0.571	0.557	0.571	0.570	0.564	0.571	**0.603**	0.575	0.577
Monahan Flat	121	0.276	0.273	0.275	0.274	0.274	0.277	0.275	**0.284**	0.276
Monument Creek	405	0.407	0.401	0.406	0.405	0.404	0.409	0.413	0.406	**0.418**
Mt. Ryan	194	0.604	0.595	0.604	0.601	0.599	0.605	**0.624**	0.604	0.601
Munson Ridge	383	0.608	0.597	0.606	0.604	0.602	0.610	**0.624**	0.611	0.611
Tokositna Valley	253	0.177	0.171	0.174	0.172	0.170	0.172	**0.176**	0.172	0.171
Upper Nome Creek	283	0.416	0.398	0.418	0.420	0.410	0.416	**0.477**	0.421	0.416
Mean	214	0.445	0.436	0.445	0.444	0.440	0.446	**0.465**	0.445	0.445

Where the column of the number tagged by bold font represents the dielectric model with the best R in that station or mean.

4.3. A Global Intercomparison between Mironov 2009 and Mironov 2019

Mironov 2009 and Mironov 2019 were selected as the representatives for mineral- and organic-soil-based dielectric models and were then compared with each other at the global scale using one-week SMAP observations from July 2, 2018, to July 8, 2018. The one-week SM retrievals of Mironov 2009 and Mironov 2019 were analyzed over more regions with abundant SOM and were also used to acquire performance clues for applying Mironov 2019 in mineral soils.

According to **Figure 6a and b**, satellite-based SM data are usually unavailable in many areas characterized by organic-rich soils likely owing to dense boreal forests, harsh surface roughness, as well as permanently frozen soils on the land surface [11,36]. The magnitude difference between Mironov 2009 and Mironov 2019 yielded SM retrievals are commonly above 0.05 m^3/m^3 generally when SOM is over 10% (**Figure 6b and e**). In the case of extreme dryness (SM < 0.1 m^3/m^3) over mineral soils (SOM < 5%), SM retrievals from Mironov 2019 are likely lower than those from Mironov 2009. As illustrated in **Figure 6d**, there is a limb where SM retrievals of Mironov 2019 are nearly constant while those from Mironov 2009 vary, possibly because of soil texture.

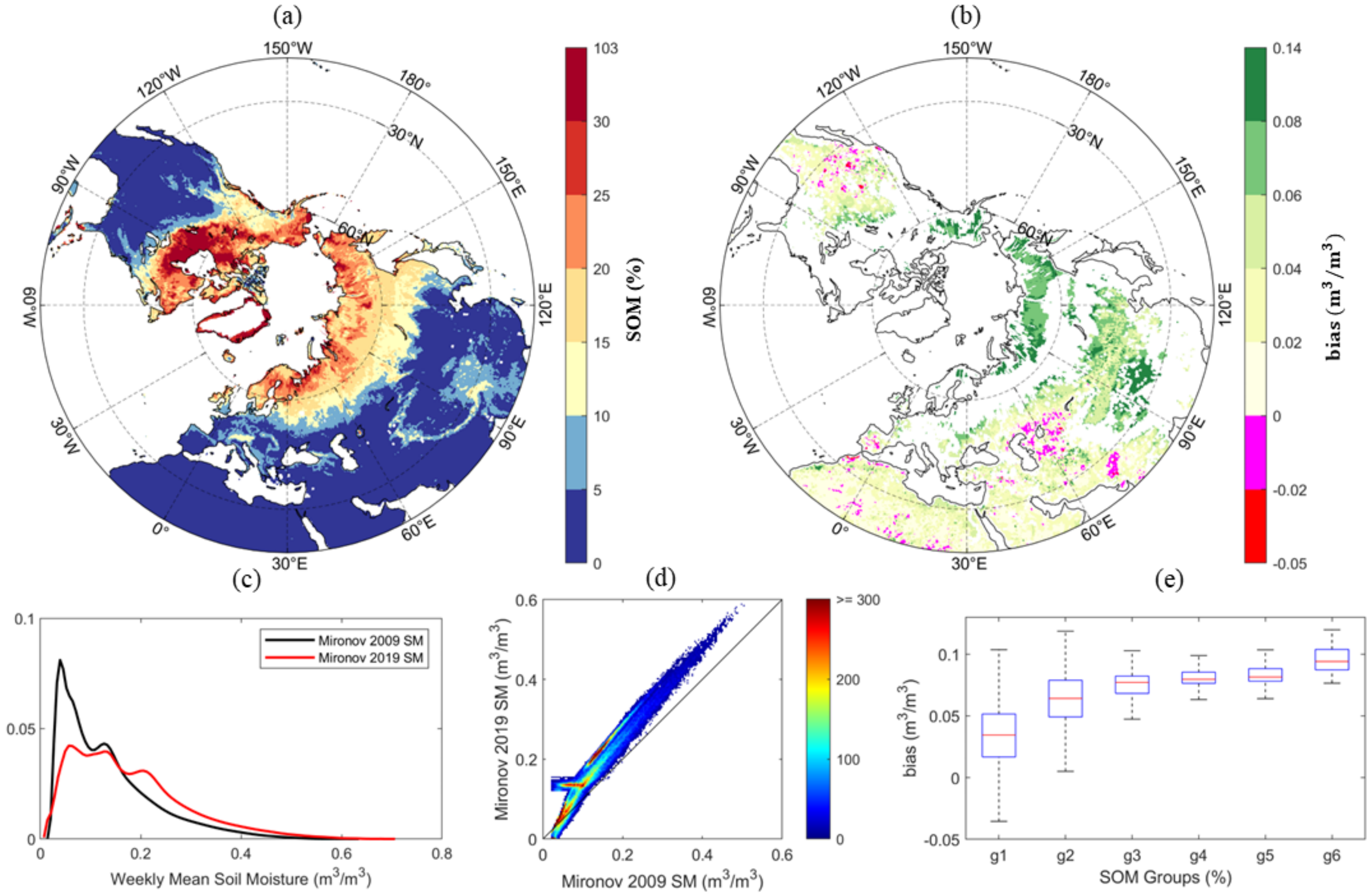

Figure 6. A global intercomparison of soil moisture retrievals from Mironov 2009 and Mironov 2019 where (a) the spatial distribution of soil organic matter (SOM) in a north polar view, (b) the spatial distribution of mean differences between soil moisture estimations using Mironov 2009 and Mironov 2019 (bias = $SM_{Mironov2019} - SM_{Mironov2009}$), (c) the probability distribution function of weekly mean soil moistures derived using the above two models, (d) the scatterplot of soil moisture using both models across the globe, and the color bar shows the number of pixels, and (e) the boxplot that describes the bias variations along with the increase of SOM that was already organized into 6 groups (g1 - g6). The organic range of each group is 0% - 5% (g1), 5% - 10% (g2), 10% - 15% (g3), 15% - 20% (g4), 20% - 30% (g5), and > 30% (g6).

4.4. Discussion

4.4.1. The Applicable Range of Dielectric Models

Although the above validation results over in-situ sites in Alaska demonstrated slightly better performance of Mironov 2019 over other models, it may be not the best model across all landscapes and climatic conditions. The accuracy of a dielectric model heavily depends on its respective applicable range. A dielectric model is likely to acquire a better performance score when being applied over samples used to develop it. In other scenarios, potential degradation of the model skills can be expected. For instance, when Dobson 1985 is adopted in soils that fall beyond the prototypal soils on which Dobson 1985 was established, some unrealistic dielectric constants could be yielded [14]. According to SMAP configurations and parameters, the frequency is confined to 1.4 GHz while most pixels in Alaska show SOM values spanning from 15% to 30%. However, it should be noted that Mironov 2019 is designed for the surface soil layer with SOM ranging from 35% to 80% [23]. Meanwhile, the natural log calibration function from [11] is proposed for highly organic soils and Decagon 5TE (in-situ sensor) which is operated at 70 MHz. Such imperfect alignments between the applicable ranges of dielectric models and the actual settings are surprisingly common, possibly leading to underestimations of the quality of these dielectric models.

4.4.2. Organic-Soil-Based Dielectric Models

Similar to other empirical dielectric models [37-42] accounting for the influence of SOM, SOM itself is not treated as a necessary input in Bircher 2016 to derive the dielectric constants of organic soils. Mironov 2019, however, incorporates the dielectric impacts of SOM and soil bulk density while omitting the clay fraction. In contrast, Park 2019 and Park 2021 consider both mineralogy and SOM. Though comprehensive, the confidence in representing the dielectric interactions among various soil properties and the quality of those global-scale soil databases greatly limit the practical uses of Park models. For example, SOM as the most critical index to classify mineral and organic soils was estimated by multiplying SOC content with a fixed factor of 1.724 [23,43]. However, the conversion factor between SOC and SOM is unlikely a global constant while [43] pointed out that this conversion factor would vary from 1.4 to 2.5 across different geographical regions.

4.4.3. Limitations of in-situ Benchmarks

Besides the limits of the model applicable range and the quality of input data sets of soil properties, the other critical factor that directly affects the assessment results is the quality of the benchmarks, i.e., in-situ SM measurements. As mentioned, breaks, missing values, and jumps were commonly found during the examination of in-situ SM time series. Furthermore, many calibration functions used to deduce in-situ SM values are designed for mineral soils only due to the unavailability of organic-soil-based calibration functions over those regions. As a result, in-situ SM values might have an underestimation issue. Despite those, at this time, these data sets might be the most practical sources to support running those dielectric models at a wide spatial coverage whilst in-situ SM observations still provide the most reliable volumetric moisture information of surface soils.

4.4.4. Characteristics of Park Models

Compared to other conventional semi-empirical dielectric models [12,16,19,21-23], Park models describe the fractions of bound water and free water differently [16,22,24]. First, Park models use the wilting point as the beginning point where free water starts to occur whereas other models set that value using an independent term named maximum bound water fraction. When the volumetric SM is between the maximum bound water fraction and porosity, most dielectric models fix the bound water content and the dielectric contribution of bound water. However, in the same SM range, Park models assume that the content of bound water and free water alters with the volumetric SM. Specifically, SM is treated as a weighted summation of the bound water and free water, where the sum of the weights of bound water (w_b) and free water (w_f) is constrained as one. It is assumed that w_b is one when SM is equal to wilting point. On the contrary, w_b declines to zero when SM reaches porosity.

According to **Figure 3e and f**, there are a few rapid drops in the curves of Park 2019 and Park 2021 when SOM exceeds 60%. Such scenarios could be explained by the wilting-point and porosity calculation equations used in Park 2019 and Park 2021. As shown in **Figure S3**, the porosity equation of Park 2019 could lead to a porosity greater than 1m^3/m^3 when SOM ranges from 30% to 35%. Meanwhile, in Park 2019, the derived wilting point could surpass the porosity when SOM is over 60%. Although the above issues have been substantially mitigated for Park 2021 with valid magnitudes of its derived porosity and wilting point, an evident bending near the wilting point could still be observed in its simulated T_B curves at highly organic soils. Therefore, caution should be paid when applying Park 2019 and Park 2021 over organic-rich soils.

4.4.5. Selection of A Globally Optimal Combination of Dielectric Models

The development of a universal dielectric model outperforming other models across all possible conditions may be overambitious. Even if such a model exists, the uncertainty of the global-scale products of soil inputs will restrict its performance. Overall, the combined use of Mironov 2009 and Mironov 2019 in the SMAP SCA-V algorithm would be a preferred option. Although comparable skills of different dielectric models have been observed, the suggestion of employing Mironov 2009 and Mironov 2019 separately for mineral and organic soils was made on account of the following reasons: 1) The input parameters of those models are the major factors affecting the dielectric constants of the soil media while without introducing excessive uncertainties [35,44]; 2) Mironov 2009 and Mironov 2019 were both built on the physical-based dielectric mixing frame, and their parameters were then adjusted by fitting the model predictions with laboratory measurements, thereby more applicable in reality; 3) Their greater accuracy has been identified based on a previous study [45] and the results exhibited here.

However, it seems that there is no rigorous set of rules about a SOM threshold used to distinguish the mineral and organic soils. [23] states that the soil can be categorized into organic soil if SOM is more than 20% whereas [46] and [47] declare that organic soil should at least contain SOM of 30% [11]. According to the results of synthetic experiments, a SOM of 15% might be an optimal threshold for distinguishing the soil types as the T_B curves of different models are closely clustered and the divergence between mineral- and organic-soil-based models seems to start after SOM exceeding 15% (**Figure 3**). Such a threshold conforms to [48] that classifies soils into organic soil or highly organic soil when SOM is more than 15%.

5. Conclusions

In this study, the skills of nine dielectric models over organic soil in Alaska have been evaluated and compared in the context of the SMAP SCA-V algorithm. Four out of nine models carefully account for the SOM effect on the complex dielectric constant of the soil-water mixtures while the remaining models were designed for use in mineral soils. The dielectric responses (expressed in a form of T_B) of those models to the increasing SOM were comprehensively investigated through artificially controlling input values. At a given SM over 0.1 m^3/m^3 and SOM higher than 15%, the simulated T_B values from organic-soil-based dielectric models are greater than those estimated from mineral-soil-based dielectric models. In other words, relative to mineral-soil-based dielectric models, organic-soil-based models are inclined to obtain higher SM estimates from the identical observed radiations. Furthermore, a SOM threshold of 15% was suggested for the separate use of mineral- and organic-soil-based dielectric models in the retrieval algorithm as the divergence of T_B curves of mineral- and organic-soil models was observed when SOM exceeds 15%.

The predictive power of each dielectric model is represented by several statistic metrics computed by comparing its SM retrievals with in-situ measurements. Compared to satellite products reflecting SM variations over a large spatial extent, in-situ point-based SM measurements exhibited more temporal variability. Additionally, even over the same place, the annual correlations between satellite-based SM retrievals and in-situ data would fluctuate a lot. Consistent with the results from synthetic experiments, organic- and mineral-soil-based models tended to induce wet and dry biases. In an integrated evaluation, Mironov 2019 presented a slightly but consistently better performance over other dielectric models, which showed a mean ubRMSE of 0.0507 m^3/m^3 and a mean R of 0.465.

Furthermore, an inter-comparison between SM retrievals within a one-week time interval from mineral- and organic-soil-based dielectric models was conducted at a global scale. Such a comparison would be useful to capture clues about the performance of organic-soil-based models over mineral soils. Mironov 2009 and Mironov 2019 were elected as the representatives of mineral- and organic-soil-based models, respectively. As a result, SM estimates from Mironov 2019 were at least 0.05 m^3/m^3 higher than those from Mironov 2009. When SM is below 0.1 m^3/m^3, SM retrievals from Mironov 2019 were occasionally smaller than SM retrievals from Mironov 2009 in mineral soils.

It should be noted that the performance of each dielectric model heavily depends on its designed application range, the quality of input data sets, as well as the accuracy of in-situ benchmarks. Different assessment results might be obtained with the update of dielectric models, in-situ measurements, and soil parameters. As such, a routine evaluation study that incorporates all the potential dielectric models and the most recent soil auxiliary data sets is recommended. In an integrated consideration of model inputs, the model physical foundation, and the practical accuracy, the separate use of Mironov 2009 and Mironov 2019 in the SMAP SCA-V algorithm for mineral soils (SOM $<$ 15%) and organic soils (SOM $\geq$ 15%) would be the optimal option at this time. Considering the SOM magnitudes at the 36 km scale, developing a sophisticated dielectric model accounting for variable SOM from 10% to 30% is expected for passive microwave remote sensing of SM.

Supplementary Materials: The following supporting information can be downloaded at: www.mdpi.com/xxx/s1, Figure S1: title; Table S1: title; Video S1: title.

Author Contributions: Conceptualization, R.Z, S.C., R.B. and V.L.; methodology, R.Z., S.C., and R.B..; data analysis, R.Z. and S.C.; writing—original draft preparation, R.Z.; writing—review and editing, S.C., R.B. and V.L. All authors have read and agreed to the published version of the manuscript.

Funding: This investigation is funded as a university subcontract under the NASA Making Earth System Data Records for USE in Research Environments (MEaSUREs) Program.

Data Availability Statement: Publicly available datasets were analyzed in this study. SMAP L2 data were downloaded from National Snow and Ice Data Center (https://nsidc.org/data/data-access-tool/SPL2SMP/versions/8, access date: April 14th, 2022). In-situ soil moisture measurements were freely available on the Natural Resources Conservation Service (NRCS), the National Water and Climate Center (NWCC) homepage (https://www.nrcs.usda.gov/wps/portal/wcc/home, access date: April 7th, 2022), and the International Soil Moisture Network (ISMN) (https://ismn.earth/en/networks, access data: April 10th, 2022), respectively.

Acknowledgments: We thank Dr. Chang-Hwan Park (Ajou University) for providing his model scripts with detailed explanations. We are also grateful to all contributors to the data sets used in this study.

Conflicts of Interest: The authors declare no conflict of interest.

Appendix A

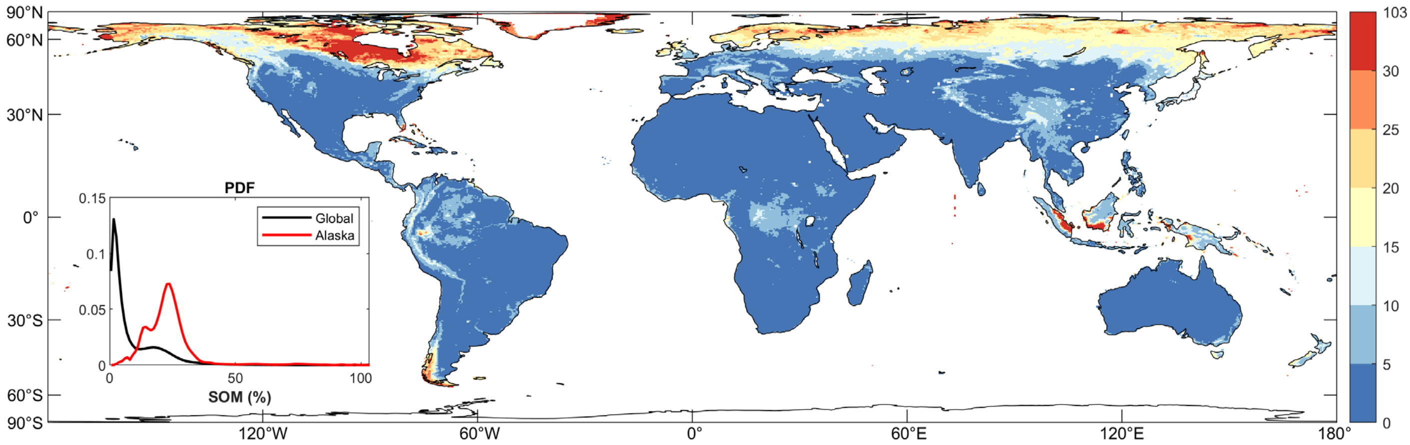

Figure A1. Global distribution of soil organic matter (SOM) where the inset describes the probability distribution function (PDF) of SOM at the global scale and in Alaska.

References

1. Njoku, E.G.; Entekhabi, D. Passive microwave remote sensing of soil moisture. *Journal of hydrology* **1996**, *184*, 101-129.
2. De Jeu, R.A.; Wagner, W.; Holmes, T.; Dolman, A.; Van De Giesen, N.; Friesen, J. Global soil moisture patterns observed by space borne microwave radiometers and scatterometers. *Surveys in Geophysics* **2008**, *29*, 399-420.
3. Kerr, Y.H.; Waldteufel, P.; Wigneron, J.-P.; Martinuzzi, J.; Font, J.; Berger, M. Soil moisture retrieval from space: The Soil Moisture and Ocean Salinity (SMOS) mission. *IEEE transactions on Geoscience and remote sensing* **2001**, *39*, 1729-1735.
4. Entekhabi, D.; Njoku, E.G.; O'Neill, P.E.; Kellogg, K.H.; Crow, W.T.; Edelstein, W.N.; Entin, J.K.; Goodman, S.D.; Jackson, T.J.; Johnson, J. The soil moisture active passive (SMAP) mission. *Proceedings of the IEEE* **2010**, *98*, 704-716.
5. Chan, S.K.; Bindlish, R.; O'Neill, P.E.; Njoku, E.; Jackson, T.; Colliander, A.; Chen, F.; Burgin, M.; Dunbar, S.; Piepmeier, J. Assessment of the SMAP passive soil moisture product. *IEEE Transactions on Geoscience and Remote Sensing* **2016**, *54*, 4994-5007.
6. Colliander, A.; Jackson, T.J.; Bindlish, R.; Chan, S.; Das, N.; Kim, S.; Cosh, M.; Dunbar, R.; Dang, L.; Pashaian, L. Validation of SMAP surface soil moisture products with core validation sites. *Remote sensing of environment* **2017**, *191*, 215-231.
7. Chan, S.K.; Bindlish, R.; O'Neill, P.; Jackson, T.; Njoku, E.; Dunbar, S.; Chaubell, J.; Piepmeier, J.; Yueh, S.; Entekhabi, D. Development and assessment of the SMAP enhanced passive soil moisture product. *Remote Sensing of Environment* **2018**, *204*, 931-941.
8. Kim, H.; Wigneron, J.-P.; Kumar, S.; Dong, J.; Wagner, W.; Cosh, M.H.; Bosch, D.D.; Collins, C.H.; Starks, P.J.; Seyfried, M. Global scale error assessments of soil moisture estimates from microwave-based active and passive satellites and land surface models over forest and mixed irrigated/dryland agriculture regions. *Remote Sensing of Environment* **2020**, *251*, 112052.
9. Zhang, R.; Kim, S.; Sharma, A.; Lakshmi, V. Identifying relative strengths of SMAP, SMOS-IC, and ASCAT to capture temporal variability. *Remote Sensing of Environment* **2021**, *252*, 112126.
10. Ulaby, F.T. Radar remote sensing and surface scattering and emission theory. *Microwave remote sensing: active and passive* **1982**.
11. Bircher, S.; Andreasen, M.; Vuollet, J.; Vehviläinen, J.; Rautiainen, K.; Jonard, F.; Weihermüller, L.; Zakharova, E.; Wigneron, J.-P.; Kerr, Y.H. Soil moisture sensor calibration for organic soil surface layers. *Geoscientific instrumentation, methods and data systems* **2016**, *5*, 109-125.
12. Dobson, M.C.; Ulaby, F.T.; Hallikainen, M.T.; El-Rayes, M.A. Microwave dielectric behavior of wet soil-Part II: Dielectric mixing models. *IEEE Transactions on geoscience and remote sensing* **1985**, 35-46.
13. Zhang, R.; Kim, S.; Sharma, A. A comprehensive validation of the SMAP Enhanced Level-3 Soil Moisture product using ground measurements over varied climates and landscapes. *Remote sensing of environment* **2019**, *223*, 82-94.

14. Mironov, V.L.; Kosolapova, L.G.; Fomin, S.V. Physically and mineralogically based spectroscopic dielectric model for moist soils. *IEEE Transactions on Geoscience and Remote Sensing* **2009**, *47*, 2059-2070.
15. Wigneron, J.-P.; Jackson, T.; O'neill, P.; De Lannoy, G.; de Rosnay, P.; Walker, J.; Ferrazzoli, P.; Mironov, V.; Bircher, S.; Grant, J. Modelling the passive microwave signature from land surfaces: A review of recent results and application to the L-band SMOS & SMAP soil moisture retrieval algorithms. *Remote Sensing of Environment* **2017**, *192*, 238-262.
16. Park, C.H.; Montzka, C.; Jagdhuber, T.; Jonard, F.; De Lannoy, G.; Hong, J.; Jackson, T.J.; Wulfmeyer, V. A dielectric mixing model accounting for soil organic matter. *Vadose Zone Journal* **2019**, *18*, 190036.
17. O'neill, P.; Jackson, T. Observed effects of soil organic matter content on the microwave emissivity of soils. *Remote sensing of environment* **1990**, *31*, 175-182.
18. O'Neill, P.; Bindlish, R.; Chan, S.; Chaubell, J.; Colliander, A.; Njoku, E.; Jackson, T. Algorithm Theoretical Basis Document Level 2 & 3 Soil Moisture (Passive) Data Products, revision G, October 12, 2021, SMAP Project, JPL D-66480, Jet Propulsion Laboratory, Pasadena, CA. . Available online: https://nsidc.org/sites/nsidc.org/files/technical-references/L2_SM_P_ATBD_rev_G_final_Oct2021.pdf (accessed on
19. Wang, J.R.; Schmugge, T.J. An empirical model for the complex dielectric permittivity of soils as a function of water content. *IEEE Transactions on Geoscience and Remote Sensing* **1980**, 288-295.
20. Peplinski, N.R.; Ulaby, F.T.; Dobson, M.C. Dielectric properties of soils in the 0.3-1.3-GHz range. *IEEE transactions on Geoscience and Remote sensing* **1995**, *33*, 803-807.
21. Mironov, V.; Kerr, Y.; Wigneron, J.-P.; Kosolapova, L.; Demontoux, F. Temperature-and texture-dependent dielectric model for moist soils at 1.4 GHz. *IEEE Geoscience and Remote Sensing Letters* **2012**, *10*, 419-423.
22. Park, C.-H.; Behrendt, A.; LeDrew, E.; Wulfmeyer, V. New approach for calculating the effective dielectric constant of the moist soil for microwaves. *Remote Sensing* **2017**, *9*, 732.
23. Mironov, V.L.; Kosolapova, L.G.; Fomin, S.V.; Savin, I.V. Experimental analysis and empirical model of the complex permittivity of five organic soils at 1.4 GHz in the temperature range from− 30° C to 25° C. *IEEE Transactions on Geoscience and Remote Sensing* **2019**, *57*, 3778-3787.
24. Park, C.-H.; Berg, A.; Cosh, M.H.; Colliander, A.; Behrendt, A.; Manns, H.; Hong, J.; Lee, J.; Zhang, R.; Wulfmeyer, V. An inverse dielectric mixing model at 50 MHz that considers soil organic carbon. *Hydrology and Earth System Sciences* **2021**, *25*, 6407-6420.
25. O'neill, P.; Chan, S.; Njoku, E.; Jackson, T.; Bindlish, R.; Chaubell, J. L3 Radiometer Global Daily 36 km EASE-Grid Soil Moisture, Version 8. Soil Moisture Retrieval Data. Boulder, Colorado, USA. **2021**, doi:https://doi.org/10.5067/OMHVSRGFX38O.
26. Dorigo, W.; Xaver, A.; Vreugdenhil, M.; Gruber, A.; Hegyiova, A.; Sanchis-Dufau, A.; Zamojski, D.; Cordes, C.; Wagner, W.; Drusch, M. Global automated quality control of in situ soil moisture data from the International Soil Moisture Network. *Vadose Zone Journal* **2013**, *12*.
27. Hengl, T.; Mendes de Jesus, J.; Heuvelink, G.B.; Ruiperez Gonzalez, M.; Kilibarda, M.; Blagotić, A.; Shangguan, W.; Wright, M.N.; Geng, X.; Bauer-Marschallinger, B. SoilGrids250m: Global gridded soil information based on machine learning. *PLoS one* **2017**, *12*, e0169748.
28. Das, N.N.; O'Neill, P. Soil Moisture Active Passive (SMAP) Ancillary Data Report, Soil Attributes, August 15, 2020, JPL D-53058, Version B, Jet Propulsion Laboratory, Pasadena, CA. Available online: (accessed on
29. Schaefer, G.L.; Paetzold, R.F. SNOTEL (SNOwpack TELemetry) and SCAN (soil climate analysis network). *Automated Weather Stations for Applications in Agriculture and Water Resources Management: Current Use and Future Perspectives* **2001**, *1074*, 187-194.

30. Schaefer, G.L.; Cosh, M.H.; Jackson, T.J. The USDA natural resources conservation service soil climate analysis network (SCAN). *Journal of Atmospheric and Oceanic Technology* **2007**, *24*, 2073-2077.
31. Dorigo, W.; Wagner, W.; Hohensinn, R.; Hahn, S.; Paulik, C.; Xaver, A.; Gruber, A.; Drusch, M.; Mecklenburg, S.; van Oevelen, P. The International Soil Moisture Network: a data hosting facility for global in situ soil moisture measurements. *Hydrology and Earth System Sciences* **2011**, *15*, 1675-1698.
32. Dorigo, W.; Himmelbauer, I.; Aberer, D.; Schremmer, L.; Petrakovic, I.; Zappa, L.; Preimesberger, W.; Xaver, A.; Annor, F.; Ardö, J. The International Soil Moisture Network: serving Earth system science for over a decade. *Hydrology and earth system sciences* **2021**, *25*, 5749-5804.
33. Entekhabi, D.; Reichle, R.H.; Koster, R.D.; Crow, W.T. Performance metrics for soil moisture retrievals and application requirements. *Journal of Hydrometeorology* **2010**, *11*, 832-840.
34. Hallikainen, M.T.; Ulaby, F.T.; Dobson, M.C.; El-Rayes, M.A.; Wu, L.-K. Microwave dielectric behavior of wet soil-part 1: Empirical models and experimental observations. *IEEE Transactions on Geoscience and Remote Sensing* **1985**, 25-34.
35. Mialon, A.; Richaume, P.; Leroux, D.; Bircher, S.; Al Bitar, A.; Pellarin, T.; Wigneron, J.-P.; Kerr, Y.H. Comparison of Dobson and Mironov dielectric models in the SMOS soil moisture retrieval algorithm. *IEEE Transactions on Geoscience and Remote Sensing* **2015**, *53*, 3084-3094.
36. Yi, Y.; Kimball, J.S.; Chen, R.H.; Moghaddam, M.; Miller, C.E. Sensitivity of active-layer freezing process to snow cover in Arctic Alaska. *The Cryosphere* **2019**, *13*, 197-218.
37. Topp, G.C.; Davis, J.; Annan, A.P. Electromagnetic determination of soil water content: Measurements in coaxial transmission lines. *Water resources research* **1980**, *16*, 574-582.
38. Roth, C.; Malicki, M.; Plagge, R. Empirical evaluation of the relationship between soil dielectric constant and volumetric water content as the basis for calibrating soil moisture measurements by TDR. *Journal of Soil Science* **1992**, *43*, 1-13.
39. Paquet, J.; Caron, J.; Banton, O. In situ determination of the water desorption characteristics of peat substrates. *Canadian Journal of Soil Science* **1993**, *73*, 329-339.
40. Skierucha, W. Accuracy of soil moisture measurement by TDR technique. *International agrophysics* **2000**, *14*.
41. Kellner, E.; Lundin, L.-C. Calibration of time domain reflectometry for water content in peat soil. *Hydrology Research* **2001**, *32*, 315-332.
42. Malicki, M.; Plagge, R.; Roth, C. Improving the calibration of dielectric TDR soil moisture determination taking into account the solid soil. *European Journal of Soil Science* **1996**, *47*, 357-366.
43. Pribyl, D.W. A critical review of the conventional SOC to SOM conversion factor. *Geoderma* **2010**, *156*, 75-83.
44. Dente, L.; Su, Z.; Wen, J. Validation of SMOS soil moisture products over the Maqu and Twente regions. *Sensors* **2012**, *12*, 9965-9986.
45. O'Neill, P.; Chan, S.; Bindlish, R.; Chaubell, J.; Colliander, A.; Chen, F.; Dunbar, S.; Jackson, T.; Peng, J.; Mousavi, M.; et al. Calibration and Validation for the L2/3_SM_P Version 8 and L2/3_SM_P_E Version 5 Data Products. *SMAP Project, JPL D-56297, Jet Propulsion Laboratory, Pasadena, CA.* **2021**.
46. Broll, G.; Brauckmann, H.J.; Overesch, M.; Junge, B.; Erber, C.; Milbert, G.; Baize, D.; Nachtergaele, F. Topsoil characterization—recommendations for revision and expansion of the FAO - Draft (1998) with emphasis on humus forms and biological features. *Journal of Plant Nutrition and Soil Science* **2006**, *169*, 453-461.
47. Zanella, A.; Jabiol, B.; Ponge, J.-F.; Sartori, G.; De Waal, R.; Van Delft, B.; Graefe, U.; Cools, N.; Katzensteiner, K.; Hager, H. European humus forms reference base. **2011**.
48. Huang, P.; Patel, M.; Bobet, A. FHWA/IN/JTRP-2008/2 Classification of Organic Soils. **2008**.